

Bubble migration in two-dimensional foam sheared in a wide-gap Couette device: Effects of non-Newtonian rheology

Hadi Mohammadigoushki^{a)}

Department of Chemical and Biological Engineering, University of British Columbia, Vancouver, British Columbia V6T 1Z3, Canada

Pengtao Yue

Department of Mathematics, Virginia Polytechnic Institute and State University, Blacksburg, Virginia 24061

James J. Feng^{b)}

Department of Chemical and Biological Engineering, University of British Columbia, Vancouver, British Columbia V6T 1Z3, Canada and Department of Mathematics, University of British Columbia, Vancouver, British Columbia V6T 1Z2, Canada

(Received 14 March 2014; final revision received 25 July 2014;
published 11 September 2014)

Synopsis

We report experiments on the migration of a large bubble in an otherwise monodisperse two-dimensional (2D) foam sheared in a wide-gap Couette device. The bubble migrates away from the walls toward an equilibrium position between the center of the gap and the inner cylinder. This differs from the situation in a narrow-gap Couette device, where the equilibrium position is at the center of the gap [Mohammadigoushki and Feng, *Phys. Rev. Lett.* **109**, 084502 (2012)]. The shift in equilibrium position is attributed to the non-Newtonian rheology of the foam, which is brought out by the non-homogeneous shearing in a wide-gap geometry. Two aspects of the rheology, shear-thinning and the first normal stress difference, are examined separately by comparing with bubble migration in a xanthan gum solution and a Boger fluid. Shear-thinning shifts the equilibrium position inward while the normal stress does the opposite. Bubble migration in the 2D foam is the outcome of the competition between the two effects. © 2014 The Society of Rheology. [<http://dx.doi.org/10.1122/1.4892660>]

I. INTRODUCTION

Foams are quintessential soft matter in that they admit both a macroscopic, continuum-based description and a microscopic, bubble-scale one. On the one hand, foam rheology is invariably measured on the bulk. In so doing, one implicitly adopts an

^{a)}Present address: Department of Chemical Engineering, University of California, Berkeley, California 94720.

^{b)}Author to whom correspondence should be addressed; electronic mail: jfeng@chbe.ubc.ca

effective-continuum view, and sometimes explicitly represents the foam rheology by continuum models [Lauridsen *et al.* (2002); Katgert *et al.* (2010)]. On the other hand, bulk flow and deformation produce changes in the microstructure, i.e., bubble-scale morphology. Shearing is known to induce neighbor-swapping rearrangements known as T1 processes [Wang *et al.* (2006); Pratt and Dennin (2003)]. Additional microstructural changes include bubble coalescence, breakup, migration, and size-based segregation [Golemanov *et al.* (2008); Herzhaft (2002); Mohammadigoushki and Feng (2012, 2013); Mohammadigoushki *et al.* (2012)]. Since foams can be examined on both levels, and indeed manifest a clear link between their microstructure and bulk flow behavior, they are excellent model systems for studying the coupling between the microscopic and macroscopic scales.

We are only beginning to understand the interaction between the two length scales, and many questions remain to be answered. Even the shear viscosity of a foam is not well understood. In one simple-shear experiment, Golemanov *et al.* (2008) observed a marked increase of the shear stress in time after the start of shear and attributed it to the breakup of the bubbles. In another experiment, Herzhaft (2002) reported a shear stress that gradually declines in time. The microstructural change underlying this decline is unclear at present. In addition, foams show shear-thinning, which can be fitted to the continuum Herschel-Bulkley model [Lauridsen *et al.* (2002); Katgert *et al.* (2010)]. The bubble velocity profile, however, differs appreciably from that predicted by the continuum model [Katgert *et al.* (2010)]. This has been ascribed to a nonlocal effect arising from the cooperative movement of bubbles within a certain “co-operativity” length scale. Surface tension is also known to produce normal stress differences on the macroscopic scale [Gardiner *et al.* (2000); Labiausse *et al.* (2007)]. Thus, the micro-macro connection is complex for foams, and their dynamics is influenced by continuum rheology as well as textural granularity.

We have been investigating one aspect of this connection, the cross-streamline migration of bubbles in sheared “two-dimensional” (2D) foam, which is a bubble raft floating on a soapy solution [Mohammadigoushki and Feng (2012, 2013)]. The two-dimensionality affords direct visualization of bubble-scale microstructures that would be impossible for 3D foams. Recent experiments in simple shear demonstrated that bubbles migrate laterally in sheared polydisperse foams and segregate according to size. Moreover, the segregation can be understood using a simple continuum model in which the smallest bubbles are viewed as an effective Newtonian fluid that suspends the larger bubbles [Mohammadigoushki and Feng (2012, 2013)]. Such a model can account for the segregation data quantitatively by combining shear-induced migration of individual bubbles with an effective diffusion due to collision among large bubbles. This adds to the collection of foam behavior that can be described as continuumlike. In the mean time, the discreteness of the bubbles manifests itself as well, in terms of “quantized” steps of migration and thresholds in shear-rate and bubble size ratio under which no migration takes place. Note that the above has been observed in simple shear in a narrow-gap Couette device.

The experiments to be presented here extend the previous work by examining bubble migration in 2D foams under nonuniform shear in a wide-gap Couette device. Now two new factors arise that may influence the bubble migration: The variation of shear rate across the gap and curvature of the streamlines. However, accounting for these in the continuum model fails to predict the experimental outcome. This simple change of geometry, as it turns out, brings out the *non-Newtonian rheology* of the foam to bear on the migration of bubbles. The novelties of the study are two. First, we present an intriguing example of the bulk rheology of the foam affecting its microstructural evolution. As far

as we know, no similar process has been reported before. Second, we demonstrate that the continuum analogy can be maintained if we view the smaller bubbles as constituting an effective non-Newtonian fluid that shows shear-thinning and normal stress difference under shear. In fact, drop migration in non-Newtonian fluids, a subject that has received long-standing attention [Gauthier *et al.* (1971); Chan and Leal (1979, 1981)], will be a key to understanding bubble migration in foam in wide-gap Couette geometry. Thus, our results suggest that certain aspects of 2D foam dynamics can be interpreted from a continuum standpoint, while others require accounting explicitly for the granularity of the bubbles [Katgert *et al.* (2010)].

II. MATERIALS AND METHODS

Our experiments focus on the lateral migration of individual large bubbles in a bubble raft made of monodisperse smaller bubbles. The main conclusion is that the smaller bubbles can be viewed as a shear-thinning, viscoelastic fluid in accounting for the lateral migration of the larger bubbles. Toward this goal, we have carried out two types of experiments: Bubble-migration experiments and rheological measurements. These are done in 2D foams as well as in polymer solutions whose rheology has been designed to mimic that of the foam.

Migration experiments are conducted in a modified Couette device of coaxial cylinders. A schematic of the experimental setup is shown in Fig. 1. The radius of the inner cylinder is $R_i = 81$ mm and that of the outer cylinder is $R_o = 99$ mm, with a gap size of $d = R_o - R_i = 18$ mm. To make a monodisperse 2D foam with a certain bubble size, we use a micro-syringe to inject nitrogen gas into a surfactant solution at precisely controlled flow rates. The characteristics of the soap solution are similar to what Mohammadigoushki and Feng (2012) have reported before. To prevent slippage at the solid surfaces, triangular teeth are machined onto the inner and outer cylinders. The surfactant solution has a viscosity $\eta_s = 50$ mPa s, density $\rho = 1200$ kg/m³, and a surface tension $\sigma = 25$ mN/m. The surfactant concentration of 5 wt. % is several times higher than the critical micelle concentration [Mohammadigoushki and Feng (2012)].

Rheological measurements are performed on commercial rheometers (Malvern Kinexus and Anton Paar MCR 502) with the bob-cup and cone-plate fixtures. Measuring

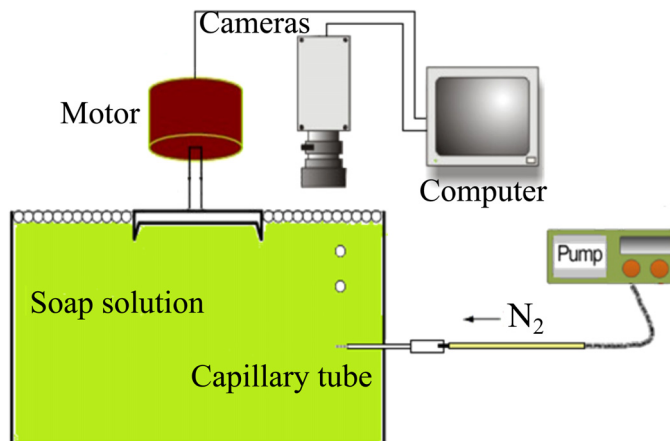


FIG. 1. Schematic of the wide-gap Couette device used in this work (not to scale). The inner cylinder is driven by a stepping motor, and the trajectory of large bubbles are tracked by three cameras at different azimuthal positions along the gap.

the shear viscosity of the 2D foam is a delicate task. We glue sandpaper onto the surfaces of the fixtures to prevent wall-bubble slip [Khan *et al.* (1988); Golemanov *et al.* (2008)]. Since our 2D foam floats on a liquid bath, we need a separate measurement without the foam such that the liquid contribution to the torque may be subtracted. Then the shear viscosity of the foam can be obtained. Typically, it takes minutes for the shear stress of the foam to stabilize into a steady-state value at a prescribed shear rate. A shear-rate sweep lasts for some 40 min, during which the foam remains stable without coarsening or bursting. The normal stress difference of 2D foam would be even more difficult to measure, and to our knowledge no such measurements have been reported in the literature. We have decided not to attempt this in our experiment.

We have also performed migration experiments and rheological measurements in aqueous solutions of xanthan gum and a Boger fluid. The xanthan solutions are made by dissolving xanthan gum polymer (West Point Naturals) in deionized water with 5 wt. % of surfactant (Sunlight by Unilever). The xanthan concentration ranges from 1000 to 4000 ppm. Our Boger fluid is a 300 ppm solution of polyacrylamide (Sigma-Aldrich, $M_w = 5\,000\,000\text{--}6\,000\,000$) in a glycerin-based high-viscosity solvent, which consists of 90 wt. % glycerin (Fisher Scientific), 9 wt. % deionized water, and 1 wt. % of surfactant. The xanthan solutions are shear-thinning with negligible normal stress, while the Boger fluid exhibits normal stress with a roughly constant viscosity. The surface tension of the Boger fluid is 36.5 mN/m, and those of the xanthan solutions fall between 32 and 34 mN/m. In all the fluids used, the surfactant level is chosen to be high enough to maintain bubble stability against coarsening and burst for at least 1 h. The surfactants do not modify the rheology of the solutions to a measurable degree.

The trajectory of bubbles is tracked using an array of three CCD cameras arranged in roughly equal spacing around the circular gap. Each camera is equipped with a 55 mm lens that allows us to measure the position of the bubble centroid and the bubble diameter with a maximum error of ± 0.02 mm. This level of uncertainty applies to all the data presented in the rest of the paper and is indicated by error bars in select plots.

III. EXPERIMENTAL RESULTS

We have performed two series of experiments—bubble-migration and rheological measurements—on three types of media: 2D foams, xanthan gum solutions, and a Boger fluid. In the following, we present the result of each experiment in turn.

A. Bubble migration in foam

The experimental protocol for recording bubble migration across streamlines is similar to that used in narrow-gap Couette cells [Mohammadigoushki and Feng (2012)]. We make a monodisperse foam consisting of bubbles of radius $r = 0.36$ mm, which covers the entire wide gap of the Couette device in a more or less regular hexagonal lattice. The foam quality, defined as the area fraction of the bubbles, is maintained at 85% for all the experiments to be presented. We then insert a single large bubble of radius R into the foam at different initial positions, and shear the foam by rotating the inner cylinder at a constant angular velocity Ω . The foam velocity profile is measured using particle-image-velocimetry (PIV) [Mohammadigoushki *et al.* (2012)]. The two control parameters are the shear rate $\dot{\gamma}$ at the inner wall, estimated from the local slope of the velocity profile, and the bubble size ratio $\kappa = R/r$. The results to be reported cover a range of the shear rate $3.50\text{ s}^{-1} < \dot{\gamma} < 8.62\text{ s}^{-1}$. The upper bound is chosen such that the centripetal force remains negligible. The lower bound ensures complete yielding of the foam throughout

the gap. At lower shear rates, the foam may yield partially in our wide-gap Couette cell, introducing unnecessary complication to the discussion of migration. We have found it convenient to cite the shear rate $\dot{\gamma}$ in reporting experimental results; this can be conveniently converted into a capillary number by $Ca = \eta_s \dot{\gamma} R / \sigma$, with σ being the surface tension of the surfactant solution. For the large bubble we have tested five sizes: $R = 0.5, 0.6, 1, 1.4,$ and 1.8 mm, corresponding to $\kappa = 1.39, 1.67, 2.79, 3.91,$ and 5.03 .

Similar to what has been reported for the narrow-gap Couette device [Mohammadigoushki and Feng (2012)], the large bubble migrates across the flow direction if the shear rate $\dot{\gamma}$ and bubble size ratio κ are each above a threshold value. The migration is driven by a hydrodynamic force that arises from the asymmetric flow and pressure fields surrounding the deformed bubbles [Mohammadigoushki and Feng (2012, 2013)]. The migration is generally away from the walls, and the hydrodynamic driving force is greatest at the wall and diminishes toward the center. The thresholds reflect the discreteness of the foam; the hydrodynamic force has to overcome the capillary pressure in neighboring bubbles in order to move the large bubble to the next row [Mohammadigoushki and Feng (2012)]. Thus, a large bubble may migrate across one or several rows if released near the wall, but not at all if released further away from the wall. For simplicity, we will exclude such partial migration from further discussion and define the thresholds of $\dot{\gamma}$ and κ according to complete migration, i.e., migration to an equilibrium position regardless of initial positions. As in the narrow-gap Couette cell, we find the $\dot{\gamma}$ threshold to decrease with increasing κ , and the κ threshold to decrease with increasing $\dot{\gamma}$ [Mohammadigoushki and Feng (2012)]. The threshold values are comparable to those in the narrow gap. In the following, we will concern ourselves only with the dynamics above these thresholds.

Figure 2 shows the migration trajectories of bubbles of two sizes ($R = 1$ and 1.4 mm) at two different shear rates. The bubble center is indicated by S , its distance from the inner cylinder is scaled by the gap width $d = R_o - R_i$. Error bars drawn on one data set

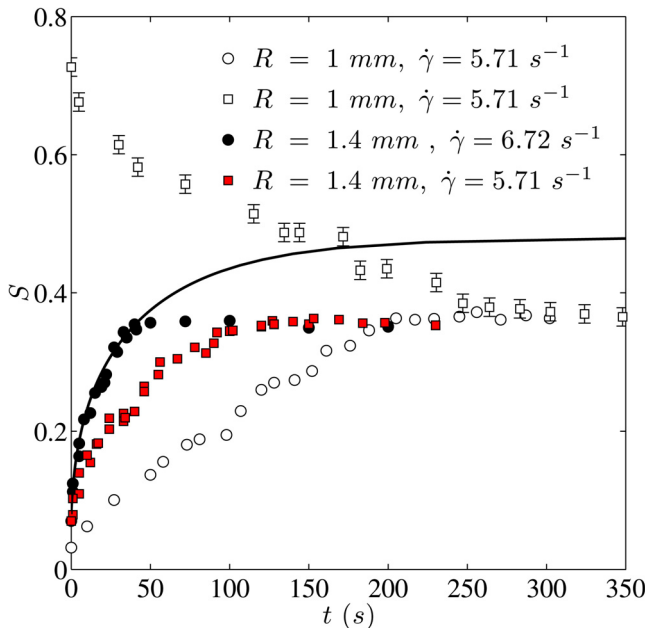


FIG. 2. Migration trajectories of bubbles of two size $R = 1$ and 1.4 mm, released from different positions in the foam sheared at two different shear rates. The curve shows the prediction of the Chan-Leal formula [Chan and Leal (1979)] for the bubble of radius $R = 1.4$ mm at $\dot{\gamma} = 5.71 \text{ s}^{-1}$.

indicate the spatial resolution in determining the bubble center. Subsequent results have similar errors and error bars will be omitted for clarity. The threshold shear rate is around 3.5 s^{-1} for the smaller bubble, and 1.5 s^{-1} for the larger one. For shear rates above this threshold, the same equilibrium position is reached from all initial positions. This equilibrium position seems to be independent of the shear rate and the bubble size ratio, although the speed of migration increases with $\dot{\gamma}$ and κ . The features described so far are similar to prior observations in the narrow-gap Couette device [Mohammadigoushki and Feng (2012)]. The key difference is that the equilibrium position is not at the center of the gap, as is the case in the narrow-gap geometry [Mohammadigoushki and Feng (2012)]. Rather it is some distance inward from the center of the gap, closer to the inner cylinder; in the particular case shown in Fig. 2, this position is at $S_e \approx 0.36$. One naturally seeks a geometrical explanation for the difference. After all, the wide-gap Couette device should produce a nonuniform shear rate profile across the gap, with higher local shear rate in the inner half of the gap than the outer half. Such asymmetry should bias the equilibrium position of the migrating bubble. This effect can be quantified with the help of the Chan-Leal theory for lateral migration of droplets in Couette flows [Chan and Leal (1979, 1981)].

Chan and Leal (1979) considered the migration of a Newtonian drop in a Newtonian matrix sheared in a Couette device, under the condition of vanishing capillary number and small drop deformation. For a bubble of radius R in a matrix of viscosity η , the dimensional migration velocity can be written as

$$v_m(S) = \frac{\sigma}{\eta} Ca^2 \left(\frac{R_i}{R_o} \right)^4 \left\{ \frac{81 R^2}{560 d^2} \left[1 + \frac{R_o^2}{(R_i + Sd)^2} \right]^2 f(S) - \frac{1}{7} \frac{R_o^4 R}{(R_i + Sd)^5} \right\}, \quad (1)$$

where $Ca = \eta \dot{\gamma} R / \sigma$ is defined using the shear rate at the inner cylinder, $f(S) = S^{-2} - (1 - S)^{-2} + 2 - 4S$, and we have put the bubble viscosity to zero. The first term in the bracket represents wall repulsion that pushes the bubble to the center of the gap ($S = 0.5$), while the second term is due to the curvature of the streamlines and drives the bubble toward the inner cylinder. Thus, the Chan-Leal formula predicts an equilibrium position between the center and the inner cylinder. Recently, we have demonstrated that this formula can be adapted to the migration of a single large bubble in a sea of monodisperse bubbles [Mohammadigoushki and Feng (2012)]. Viewing the smaller bubbles as an effective continuum, we observed experimentally that the large bubble deforms much more than in a real Newtonian fluid at the same capillary number. Interpreting this enhanced deformation as an elevated *effective capillary number* Ca^e , we have shown that the *modified* Chan-Leal formula, with Ca replaced by Ca^e , predicts the migration of the large bubble in a foam [Mohammadigoushki and Feng (2012)] and size-based bubble segregation [Mohammadigoushki and Feng (2013)] to quantitative accuracy. Applied to the conditions of one of the experimental runs of Fig. 2, the modified Chan-Leal formula gives the migration trajectory plotted as the solid curve. It predicts only a slight inward shift of the equilibrium position, to $S_e = 0.47$, which cannot account for the much larger shift observed experimentally. Therefore, the observations in the wide-gap experiment cannot be accounted for by the curvilinear geometry alone.

A factor that has not been taken into account in the above comparison is the *non-Newtonian rheology* of the foam. The Chan-Leal formula used in Fig. 2 is for a Newtonian suspending fluid. Its success with bubble migration in a foam has so far been limited to uniform shear in a narrow-gap Couette cell [Mohammadigoushki and Feng (2012, 2013)]. Can it be that the nonuniform shearing in the wide-gap device brings out non-Newtonian rheology that is not manifest in the narrow-gap Couette cell? Shear-

thinning will accentuate the nonlinearity of the velocity profile, and a large bubble would thus experience unequal viscosities upon its two sides. Moreover, the first normal stress difference N_1 would exhibit a similar asymmetry between the two sides, potentially producing a radial force. To ascertain these potential effects on bubble migration in the foam, we need to characterize the bulk rheology of the foam first. This has in turn motivated us to make polymer solutions possessing shear-thinning and elasticity separately, each mimicking one aspect of the foam rheology. Thus, bubble migration in these solutions may be investigated as benchmarks for gauging the bubble migration in foam.

B. Bulk rheology of 2D foam and polymer solutions

Foams have a yield stress, and in the fully yielded state exhibit shear-thinning and normal stress differences [Gardiner *et al.* (2000); Katgert *et al.* (2010); Kraynik and Reinelt (2004); Ovarlez *et al.* (2010)]. To probe the shear-thinning of our 2D foam, we have measured its shear rheology on a rotational rheometer using the bob-cup fixture. To accommodate a large number of bubbles, we used a wide-gap setup, with the radius of the inner cylinder being $R_i=22$ mm and that of the stationary outer cylinder being $R_o=35$ mm. For a fully yielded foam, the local shear rate at the inner cylinder is calculated from the following formula [Krieger and Elrod (1953); Estellé *et al.* (2008)]:

$$\dot{\gamma} = 2\Omega \frac{\Gamma}{1 - R_i^2/R_o^2} - \Omega \frac{1 - \Gamma}{\ln(R_i/R_o)}, \tag{2}$$

where Ω is the rate of rotation of the inner cylinder, and $\Gamma = d(\ln \Omega)/d(\ln M)$, and M being the torque on the inner cylinder.

Figure 3 shows the shear stress as a function of the shear rate for our 2D foam. Following prior experiments on 2D and 3D foams [Katgert *et al.* (2010); Ovarlez *et al.* (2010)], we fit the data by a Herschel-Bulkley model

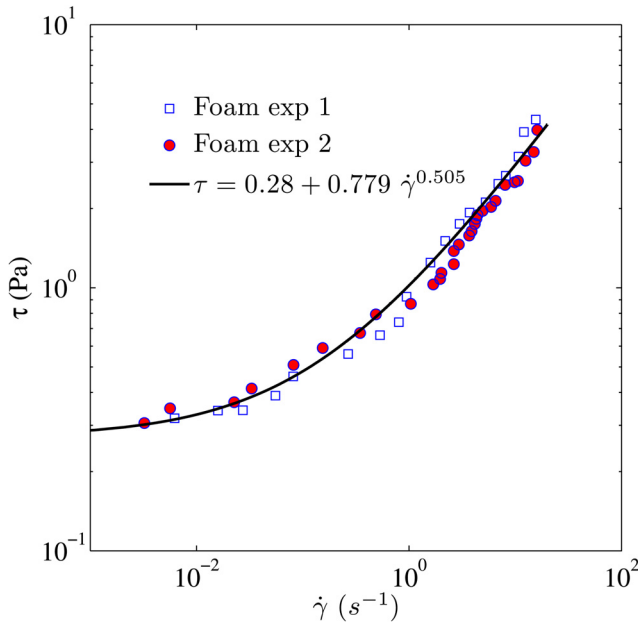


FIG. 3. Shear flow curve of the 2D foam measured in a rheometer with a bob-cup fixture. Two data sets obtained under identical conditions are plotted along with a best-fitting curve to the Herschel-Bulkley equation [Eq. (3)].

$$\tau = \tau_y + K\dot{\gamma}^n, \quad (3)$$

with a yield stress $\tau_y = 0.28$ Pa, consistency $K = 0.779$ Pa sⁿ, and a power-law index $n = 0.505$. Thus, our foam shows similar shear-thinning behavior to previous experiments [Katgert *et al.* (2010); Ovarlez *et al.* (2010)].

Although the bulk rheology of 2D foam is adequately represented by the Herschel-Bulkley model, foam dynamics is subtler than Eq. (3) might suggest. Katgert *et al.* (2010) have discovered a mismatch between global rheology and local flow behavior. For instance, the foam may flow in regions where the stress is below the yield stress τ_y . The bubble velocity profile across the gap differs from that computed from Eq. (3), and appears to be independent of the shear rate. Our own PIV measurement confirms the same effect (Fig. 4). The velocity profile, after scaling by the inner cylinder velocity $v_i = \Omega R_i$, is essentially independent of $\dot{\gamma}$, and falls considerably below the velocity profile expected from the global constitutive equation. Katgert *et al.* (2010) ascribed this discrepancy to a nonlocal effect, by which neighboring bubbles affect each other's movement in a cooperative manner. This allows the local flow to be influenced by the discreteness of the bubbles, aside from the global rheology of the foam as a whole. In the present study, we approach bubble migration mostly from an effective-continuum standpoint. But the discreteness of the foam must be borne in mind. We will return to this apparent duality in foam rheology at the end.

Both 2D and 3D foams are known to exhibit a first normal stress difference N_1 [Gardiner *et al.* (2000); Kraynik and Reinelt (2004); Labiausse *et al.* (2007); Okuzono *et al.* (1993)]. But we have not been able to measure N_1 directly for our flowing 2D foam, nor have we found any such measurements in the literature. Direct measurement of N_1 will require special instrumentation, with pressure sensors embedded flush with the outer or inner cylinders in a Couette device. The only experimental data appear to be for small-strain shearing of a 3D foam in the preyielding elastic regime [Labiausse *et al.* (2007)].

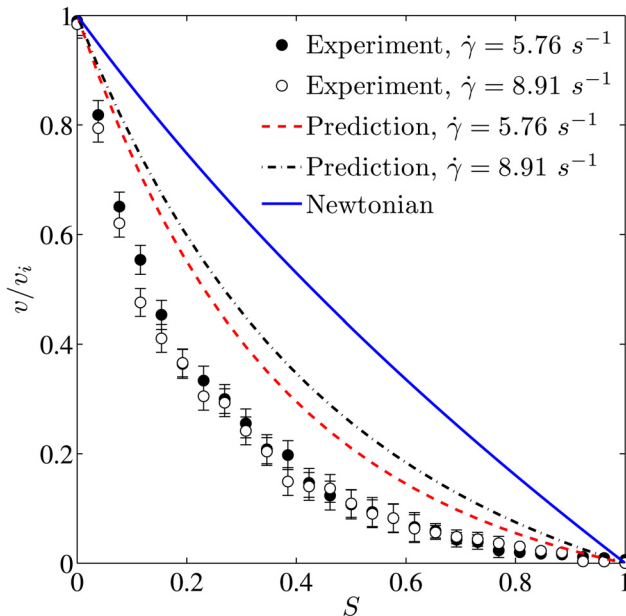


FIG. 4. Bubble velocity profiles for a monodisperse foam at two different shear rates. The velocity is scaled by $v_i = \Omega R_i$, velocity at the inner cylinder. The dash lines indicate predictions from the Herschel-Bulkley model [Eq. (3)], and a Newtonian profile is also plotted for comparison.

From numerical computations, [Kraynik and Reinelt \(2004\)](#) determined that N_1 is on the same order of magnitude as the shear stress for 3D foam before yielding. In simulations of a random 2D foam undergoing simple shear in the yielded regime, [Okuzono *et al.* \(1993\)](#) recorded N_1 values roughly twice as large as the shear stress over a range of shear rates. In view of the limited data in the literature, we have decided to use the results of [Okuzono *et al.* \(1993\)](#) as a guideline, and assume that for our 2D foam N_1 is on the same order of magnitude as the shear stress, which we have measured with confidence.

As shear-thinning and normal stress act simultaneously on bubble migration in our foam, it is impossible to identify and analyze their individual contributions. Therefore, we have sought to probe the two effects separately by using shear-thinning and visco-elastic polymer solutions that represent each aspect of the foam’s rheology. Aqueous solution of xanthan gum is known to exhibit shear-thinning but negligible elasticity [[Aytouna *et al.* \(2013\)](#); [Bonn and Meunier \(1997\)](#)]. We have tested a series of xanthan solutions and compared their viscosity to that of the foam in Fig. 5. The 2500 ppm solution approximates the foam shear viscosity most closely. Therefore, we choose this solution as the representative for the shear-thinning behavior of foam.

To represent N_1 of the foam, we have made a polyacrylamide solution as a Boger fluid. Figure 6 compares the shear rheology of the Boger fluid with that of the foam. Within the range of shear rate tested, the Boger fluid exhibits an essentially constant shear viscosity, and an N_1 that scales approximately with $\dot{\gamma}^2$. Ideally, we would have liked N_1 of the Boger fluid to match the foam shear stress in the $\dot{\gamma}$ range of interest, up to 8.62 s^{-1} . This turns out to be difficult to realize experimentally. For one, increasing the polymer concentration in the Boger fluid incurs appreciable shear-thinning. Thus, we have accepted this Boger fluid as roughly representing the order of magnitude of the normal-stress in the foam. The relaxation time of the Boger fluid can be estimated from $N_1/(2\eta\dot{\gamma}^2)$ [[Bird *et al.* \(1987\)](#)]. Thus we define a Deborah number $De = N_1/(2\eta\dot{\gamma})$.

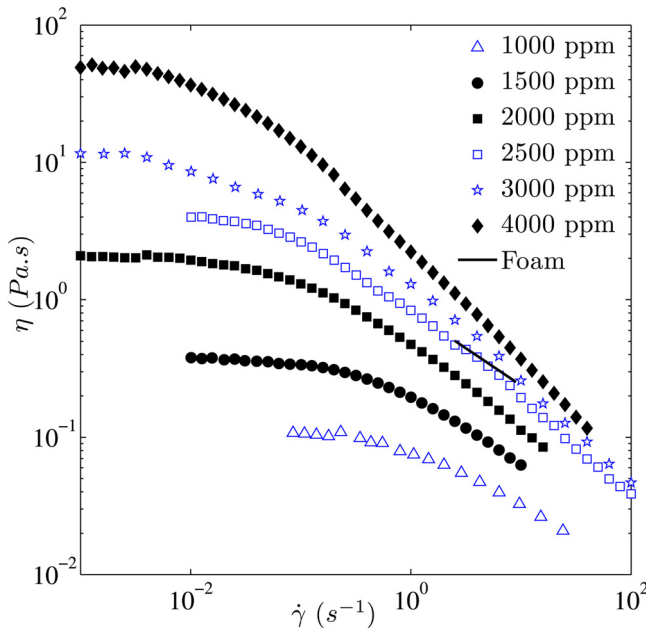


FIG. 5. Shear viscosity of xanthan gum solutions of various concentrations. The line indicates the foam viscosity in the range of shear rates used in the bubble-migration experiments. In this range, the 2500 ppm xanthan solution has a power-law viscosity $\eta = 0.85\dot{\gamma}^{-0.55}$, in unit of Pa with $\dot{\gamma}$ in s^{-1} .

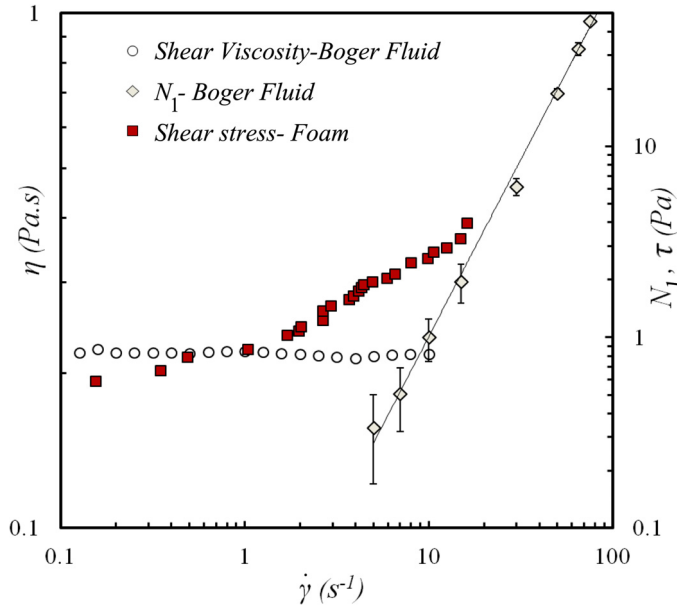


FIG. 6. Shear rheology of the Boger fluid, with circles for the shear viscosity η and diamonds for the first normal stress difference N_1 . The straight line is a power-law fitting for N_1 with a slope close to 2. The filled squares show the shear stress of the foam τ , which is comparable in magnitude to N_1 of the Boger fluid, especially near the upper bound of the shear rate.

C. Bubble migration in shear-thinning and Boger fluids

We have conducted bubble-migration experiments in the shear-thinning xanthan solution and the Boger fluid, using the same wide-gap Couette device, bubble sizes, and operating conditions as in the foam experiments. As the non-Newtonian polymer solutions represent the “effective continuum” formed by the small bubbles in our 2D foam, we release single “large” bubbles in these experiments. Figure 7 depicts migration of bubbles of two sizes in the xanthan solution at different shear rates and initial positions. Remarkably, all the runs reach essentially the same equilibrium position at $S_e \approx 0.25$, roughly midway between the center of the gap and the inner cylinder. This is much more inward than in a Newtonian fluid, in which a single bubble follows the Chan-Leal formula closely (stars and solid curve in Fig. 7), leading to an equilibrium position of $S_e = 0.47$. Besides, the speed of migration increases with the bubble size and the shear rate, but the equilibrium position does not seem to depend on either.

Thus, shear-thinning tends to shift the bubble’s equilibrium position toward the inner cylinder. This trend is consistent with the previous experimental results of [Gauthier et al. \(1971\)](#). In a wide-gap Couette device, they studied migration of a deformable droplet in a shear-thinning fluid with power-law index $n = 0.71$. Droplets of different sizes starting from different initial positions all arrive at the same equilibrium position $S_e \approx 0.4$. Our xanthan solution has stronger shear-thinning ($n = 0.45$) than their fluid, and it is reasonable that the bubbles assume a position farther inward than in their case. Regarding the hydrodynamic origin of the effect, one may imagine that the bubble experiences reduced viscosity on the side closer to the inner wall, where the shear rate is higher. We will return to this idea in Sec. IV B.

The opposite trend is observed in the Boger fluid. Figure 8 shows migration trajectories of bubbles of three sizes released from different initial positions at two shear rates. In all cases, the bubble migrates to an equilibrium position close to $S_e = 0.57$ in the outer

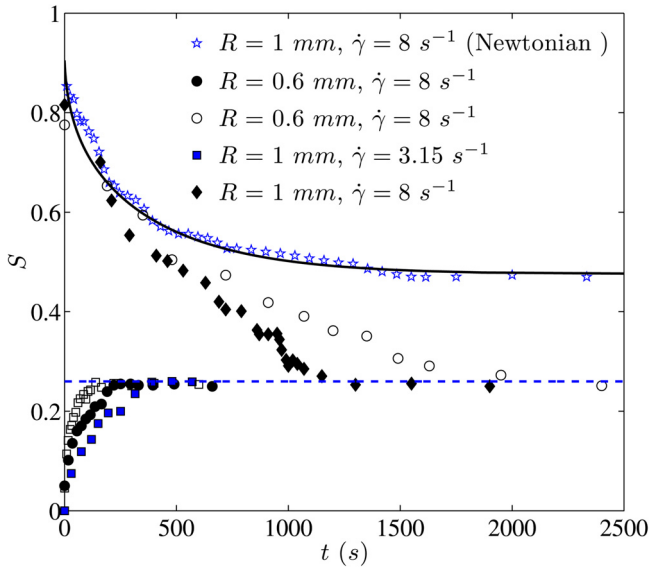


FIG. 7. Migration trajectories of bubbles in the xanthan solution starting from different initial positions. The bubbles are of two sizes ($R = 0.6$ and 1 mm) and sheared at two shear rates ($\dot{\gamma} = 3.15$ and 8 s $^{-1}$). The horizontal dashed line marks the equilibrium position. For comparison, a migration trajectory in Newtonian fluid (stars) and prediction of the Chan-Leal formula (solid curve) are also shown.

half of the gap. This suggests that the normal stress N_1 tends to force the bubble outward. Furthermore, the equilibrium position shows little dependence on the shear rate $\dot{\gamma}$ and the bubble size R , although the migration speed increases with both.

IV. ANALYSIS AND DISCUSSION

We undertake three main tasks in this section: (i) To analyze the migration of a single bubble in the Boger fluid; (ii) to analyze the migration of a single bubble in the shear-

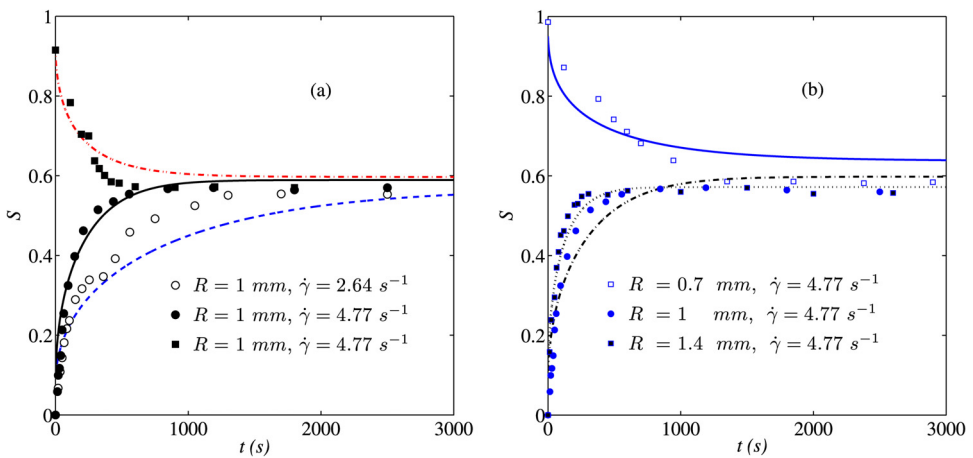


FIG. 8. Migration trajectories of bubbles in the Boger fluid. (a) A bubble of radius $R = 1$ mm released from two initial positions at two shear rates, corresponding to $(Ca, De) = (0.0156, 0.0674)$ and $(0.0282, 0.114)$. (b) The effect of bubble size at a fixed shear rate. $De = 0.114$ is independent of R , and $Ca = 0.0198, 0.0282,$ and 0.0395 for the three R values. The curves show the predictions of the Chan-Leal formula [Eq. (4)].

thinning fluid; and (iii) to rationalize the migration of a larger bubble in our 2D foam from the last two factors. Finally, we reflect on the validity of the effective-continuum analogy despite the discreteness of the foam.

A. Effect of elasticity

To analyze the migration of single bubbles in the Boger fluid, we rely heavily on the asymptotic theory of [Chan and Leal \(1979, 1981\)](#) for lateral migration of neutrally buoyant drop in a suspending fluid. This theory was developed for viscoelastic second-order fluids, with Newtonian fluids as a special case. As the second-order fluid exhibits normal stress differences but no shear-thinning, it is a fitting description of our Boger fluid. Geometrically, the theory allows for shear-rate gradients in a wide-gap Couette cell, making it relevant to the present experiments. Despite the buoyancy force, our bubbles are mostly submerged in the liquid [[Mohammadigoushki and Feng \(2012\)](#)]. Moreover, the perturbation theory requires $R/d \ll 1$, $Ca \ll 1$ and $De \ll 1$, Ca and De being the capillary number and Deborah number, respectively. These conditions are satisfied by our experiments. The Newtonian version of the theory accurately predicts bubble-migration experiments in a narrow-gap Couette cell [[Mohammadigoushki and Feng \(2012\)](#)] as well as in the current wide-gap Couette cell.

For a bubble in a Boger fluid, the Chan-Leal theory predicts a migration velocity [[Chan and Leal \(1981\)](#)]

$$v_m(S) = \frac{\sigma}{\eta} Ca^2 \left(\frac{R_i}{R_o}\right)^4 \times \left\{ \frac{81}{560} \frac{R^2}{d^2} \left[1 + \frac{R_o^2}{(R_i + Sd)^2} \right]^2 \left(1 + 0.418 \frac{De}{Ca} \right) f(S) - \frac{1}{7} \left(1 - 2.30 \frac{De}{Ca} \right) \frac{R_o^4 R}{(R_i + Sd)^5} \right\}, \quad (4)$$

where $De = N_1/(2\eta\dot{\gamma})$ is the Deborah number for the Boger fluid, and we have assumed a ratio between the normal stress differences $N_2/N_1 = -0.167$ following [Chan and Leal \(1981\)](#). Applied to our experimental conditions, the predictions of Eq. (4) are plotted as solid and dashed lines in Fig. 8. Three interesting observations can be made.

First, the formula correctly predicts the outward shift of the bubble's equilibrium position in all cases. In Fig. 8(a), the measured $S_e = 0.57$ differs from the predicted $S_e = 0.60$ by some 5%. The migration speed is overpredicted when the bubble is near the walls, probably because the theoretical v_m increases without bound toward the walls. For longer times, however, the migration velocity is underpredicted for reasons that are unclear at present. But overall there is reasonable agreement between experiment and theory. Note that in the Chan-Leal formula [Eq. (4)], the first term in the bracket accounts for wall effects that always push the drop toward the center of the gap. The second term, due to gradient of the shear rate, can change sign depending on the magnitude of the viscoelasticity (De) relative to drop deformation (Ca). For all runs in Fig. 8, De/Ca is above 2.88. Thus, the non-Newtonian N_1 effect dominates the drop-deformation effect and makes the second term positive, pushing the drop outward.

To extract a migration force from the experimental data, we differentiate the $S(t)$ curve to compute a migration velocity $v_m(S)$, and then use the Stokes formula to obtain a lateral force F_B . Figure 9(a) plots such a force for one of the trajectories in Fig. 8. As expected, F_B is large and positive close to the inner cylinder, and negative but smaller near the outer cylinder. $F_B = 0$ occurs at $S_e = 0.57$. By subtracting the lateral migration force for a Newtonian fluid F_N , computed from the Chan-Leal migration velocity [Eq. (1)] at the

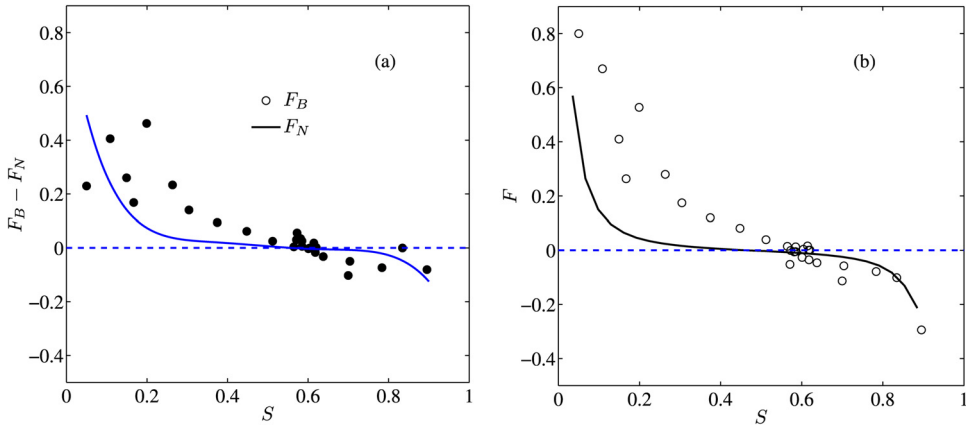


FIG. 9. The migration force in a Boger fluid, made dimensionless by $\eta\dot{\gamma}R^2$. (a) The force $F_B = 6\pi\eta Rv_m$, with the migration velocity v_m computed from the trajectory of Fig. 8 with $R = 1$ mm and $\dot{\gamma} = 4.77$ s $^{-1}$. The migration force F_N in a comparable Newtonian fluid, calculated from the Chan-Leal formula, is shown for comparison. The horizontal dashed line indicates $F = 0$. (b) The net migration force due to N_1 , $F_B - F_N$ (symbols), compared with that predicted by the Chan-Leal formula (curve).

same Ca using Stokes’ law, we can isolate the “net contribution” of the normal stress difference N_1 to the lateral migration, and such a force is plotted in Fig. 9(b). This force is in nearly quantitative agreement with the model prediction. As pointed out by Chan and Leal (1981), this net force also comprises contributions from the wall repulsion and the shear-rate gradient. The former points to the center of the gap whereas the latter points radially outward. The two balance at a position between the center and the outer wall. Heuristically, one may think of the lateral force as arising from an asymmetry between N_1 acting on the two sides of the bubble [Karnis and Mason (1966)] or from a “hoop thrust” on bowed streamlines around it [Chan and Leal (1979)].

Second, for a fixed bubble size, the formula predicts a final equilibrium position that is independent of the shear rate, in agreement with our observations. The independence of S_e on $\dot{\gamma}$ can be readily appreciated from Eq. (4). The non-Newtonian rheology affects S_e only through De/Ca , and $\dot{\gamma}$ cancels out of this ratio. This ratio represents the competition between the normal stress N_1 and the bubble deformation in lateral migration. As demonstrated by Chan and Leal (1979) in Newtonian and second-order fluids, the bubble deformation creates an asymmetry in the flow and stress fields in the vicinities, which tends to push the bubble away from solid walls. Thus, this effect opposes that of N_1 in the outer half of the Couette device. When the shear rate $\dot{\gamma}$ is elevated, N_1 increases and so does the bubble deformation. The Chan-Leal theory shows that these two effects cancel out precisely.

Third, the Chan-Leal formula predicts the equilibrium position S_e shifting away from the outer wall as the bubble size R increases relative to the gap d (Fig. 10). This is due partly to stronger wall repulsion [first term in Eq. (4)], and partly to a diminishing N_1 effect relative to an increasing Ca . This effect is stronger for smaller R/d and saturates for larger R/d . In comparison, our experimental data show a weaker effect of drop size. As R increases from 0.7 to 1.8 mm, S_e shifts inward toward the centerline, but by an amount below the roughly 10% predicted by the Chan-Leal formula. At present we have no explanation for this discrepancy. Note, however, that our current data cover a relatively narrow range of bubble size. The discrepancy needs to be examined over a wider R range in a more thorough investigation.

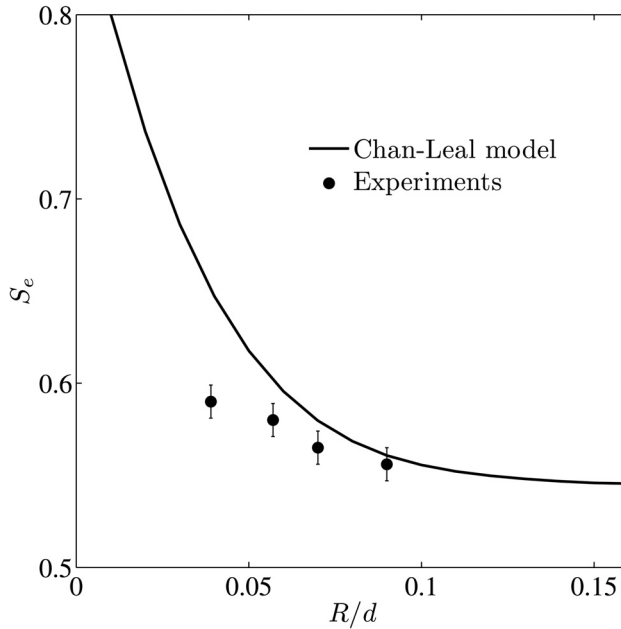


FIG. 10. The equilibrium position S_e as a function of the bubble size R/d in the Boger fluid: Comparison between experiments and the Chan-Leal formula. The error bars indicate the limit of image resolution. The conditions are identical to those of Fig. 8(b), with the shear rate fixed at $\dot{\gamma} = 4.77 \text{ s}^{-1}$.

B. Effect of shear-thinning

We have observed that shear-thinning tends to shift the equilibrium position S_e toward the inner cylinder (Fig. 7), and this trend agrees with prior experiment by [Gauthier *et al.* \(1971\)](#). To rationalize this observation, we can no longer resort to the Chan-Leal theory as it does not allow shear-thinning. But one may follow a similar physical reasoning to that employed above for the Boger fluid. We argue that the bubble is subject to two forces, one due to drop deformation in a Newtonian fluid, as given by the Newtonian version of the Chan-Leal formula, and the other due to the shear-thinning rheology. The latter force cannot be easily estimated from scaling arguments. In the following, we probe it from the experimental trajectories.

Differentiation of the bubble-migration trajectories in the xanthan solution (Fig. 7) gives us the instantaneous migration velocity at different radial positions. Figure 11(a) compares v_m from one of the trajectories (with $R = 1 \text{ mm}$ and $\dot{\gamma} = 8 \text{ s}^{-1}$) with a Newtonian curve calculated from the Chan-Leal formula using the viscosity of the xanthan solution at the middle of the gap $S = 0.5$. Even with the scatter in the data, it is clear that shear-thinning shifts the migration velocity curve downward over the entire gap. In the outer region, the inward migration is enhanced, while in the inner region, the outward migration is hindered. From the migration velocity $v_m(S)$ and the local viscosity for the xanthan solution, we can estimate a lateral migration force $F_X(S)$ from the Stokes formula. Then the difference $F_X - F_N$, with the Newtonian force F_N computed at the viscosity of the xanthan solution at the center of the gap, gives us a “net migration force” due to shear-thinning [Fig. 11(b)]. Evidently, shear-thinning gives rise to an additional lateral force that points inward throughout the gap. Despite the scatter in the data, one discerns a roughly symmetric spatial distribution of this force; it is larger near the walls, and diminishes toward the center of the gap.

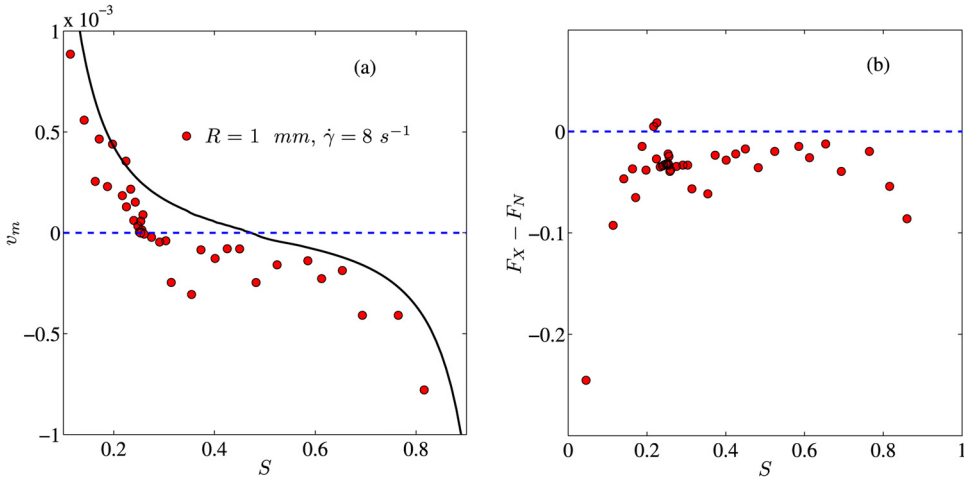


FIG. 11. (a) The migration velocity in the xanthan solution at $R = 1$ mm and $\dot{\gamma} = 8$ s $^{-1}$, scaled by the velocity at the inner cylinder $v_i = \Omega R_i$, compared with the Newtonian prediction by the Chan-Leal formula. (b) The net migration force due to shear-thinning $F_X - F_N$, scaled by $\eta\dot{\gamma}R^2$, η being the viscosity at the shear rate $\dot{\gamma}$.

Regarding the physical origin of the lateral migration force due to shear-thinning, we can only offer a vague, heuristic argument. Shear-thinning produces a difference in viscosity between the two sides of the bubble, which then creates an additional asymmetry in the flow and stress fields, and in turn a net lateral force. The viscosity is lower on the inner side of the bubble than on the outer side. One may imagine that the more viscous fluid on the outer side tends to push the bubble inward. Without a solid grasp of the lateral force, it is difficult to explain why the equilibrium position is insensitive to $\dot{\gamma}$ and R/d .

C. Migration of large bubbles in foam

Having analyzed both shear-thinning and normal-stress effects, we return to bubble migration in the 2D foam. Viewing the surrounding small bubbles as an effective continuum possessing both normal stress and shear-thinning, we rationalize the experimental observations as the outcome of the competition between the two rheological features of the foam.

The normal stress difference N_1 generates a predominantly outward force on the bubble, except near the outer wall [Fig. 9(b)], whereas shear-thinning engenders an inward force [Fig. 11(b)]. These two forces are of comparable magnitude, ranging roughly from 0.02 in the middle of the gap to 0.2 near the walls. As a leading-order approximation, we may view the bubble migration in the xanthan solution or Boger fluid as the addition of a shear-thinning or N_1 effect, respectively, on the underlying Newtonian effect. Then bubble migration in the foam can be predicted from summing the lateral forces F_N in the Newtonian fluid, $F_B - F_N$ in the Boger fluid and $F_X - F_N$ in the xanthan solution. The resulting total force $F_T = F_B + F_X - F_N$ can then be compared directly with the migration force in the foam.

To carry out such a comparison, the parameters need to be matched among the different scenarios. Using F_X of Fig. 11, at $R = 1$ mm and $\dot{\gamma} = 8$ s $^{-1}$, we calculate F_N and F_B from the Chan-Leal formula using the foam viscosity (which matches the xanthan viscosity) at the center of the gap. We happen not to have the Newtonian and Boger-fluid experiments at $R = 1$ mm and $\dot{\gamma} = 8$ s $^{-1}$, but the agreement between the Chan-Leal formula and such experiments has been established before [cf. Figs. 7 and 9(b)]. To compare

with migration in foam, an effective capillary number has to be estimated for the latter based on the bubble deformation [Mohammadigoushki and Feng (2012)]. The shear-thinning experiment has a capillary number $Ca = 0.11$, which, taken to be the effective Ca^e , corresponds to a shear rate of $\dot{\gamma} = 5.45 \text{ s}^{-1}$ for the foam. The closest foam experiment, at $R = 1 \text{ mm}$ and $\dot{\gamma} = 5.71 \text{ s}^{-1}$, is then used to estimate the lateral migration force F_F from the measured migration velocity in the foam (Fig. 2). Similar analysis has been carried out for other values of R and $\dot{\gamma}$, with essentially the same outcome.

Figure 12 shows reasonable agreement between F_T and F_F . Note that there is no fitting parameter in this comparison, and the main assumption made is the linear summation of the separate contributions to the migration force. Overall, the effective-continuum estimation F_T stays above the “true” migration force F_F in the foam. In the inner part of the gap, the outward force is overestimated, while in the outer part, the inward force is underestimated, roughly by a factor of 2 in both cases. However, $F_T = 0$ and $F_F = 0$ give essentially the same equilibrium position S_e . The general agreement in Fig. 12 suggests that bubble migration in the foam is due to the competition between its shear-thinning and normal-stress effects.

In our discussion so far, we have viewed the 2D foam of smaller bubbles as an effective continuum, a non-Newtonian fluid exhibiting shear-thinning and normal stress difference. Furthermore, the Chan-Leal theory, originally developed for drops suspended in a liquid medium, can apparently be adapted to account for bubble migration in our foam, with more or less quantitative accuracy. The success of the continuum description and that of the Chan-Leal theory are both somewhat surprising. The traditional continuum view requires a separation of length and time scales, between those of the molecular motion in the fluid and those of the macroscopic flow. In our 2D foam, on the other hand, the “large bubble” is only about twice as large as the smaller ones making up the “continuum.” This is reminiscent of the falling-ball rheometer for measuring the viscosity of a suspension, made of particles comparable in size with that of the falling ball [Brenner *et al.* (1990)].

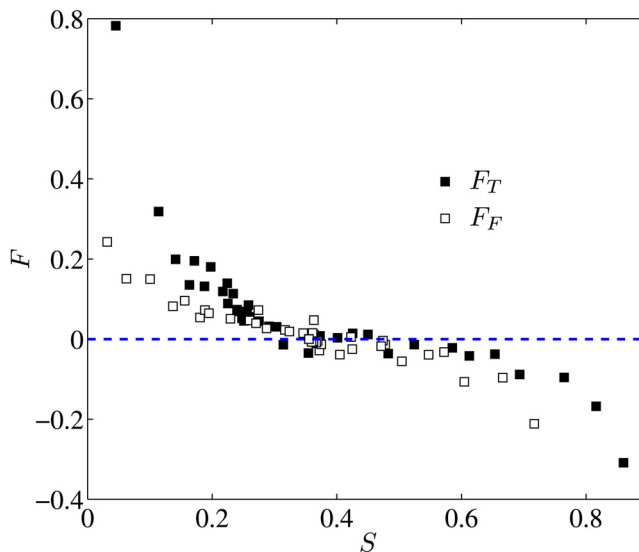


FIG. 12. Lateral migration force in the foam: Comparison between the effective-continuum prediction $F_T = F_B + F_X - F_N$, as additive sums of Newtonian [Eq. (1)], normal stress [Fig. 9(b)] and shear-thinning [Fig. 11(b)] contributions, with F_F calculated from the migration trajectory of a large bubble in the foam (Fig. 2, $R = 1 \text{ mm}$, $\dot{\gamma} = 5.71 \text{ s}^{-1}$). The forces are scaled by $\eta\dot{\gamma}R^2$.

The Chan-Leal theory requires a drop or bubble to be completely immersed in a surrounding liquid, while our bubbles float atop a soap solution. [Mohammadigoushki and Feng \(2012\)](#) have shown that surface tension keeps most of the bubble volume below the free surface. Nevertheless, the presence of the free surface should affect the viscous friction on the bubble during its migration. Moreover, the abundance of surfactants in the bulk liquid suggests near-maximum surface coverage, and Marangoni stresses may modify the boundary condition on the bubble surface and hence its migration. Indeed we have used the Stokes formula, not the Hadamard formula, in estimating the migration force on the bubbles. Despite these differences, we have confirmed that the Chan-Leal formula accurately predicts the migration of a single bubble in Newtonian and Boger fluids in narrow- and wide-gap Couette devices [cf. Fig. 1 of [Mohammadigoushki and Feng \(2012\)](#) and Fig. 8 in this paper]. Although we have used this as the basis for modifying the Chan-Leal formula for foam, we have no explanation for its “unreasonable effectiveness.”

V. CONCLUSION

In this paper, we have reported experiments on the migration of a large bubble in a monodisperse 2D foam of small bubbles sheared in a wide-gap Couette device. The nominal shear rate is varied in such a range that the entire gap is fully yielded and flowing, but inertia remains negligible. The main findings of the work can be summarized as follows:

- (a) If the shear rate and the bubble size ratio both exceed certain thresholds, the large bubble migrates radially to an equilibrium position that is independent of the initial position, the shear rate, and the bubble size ratio. The two thresholds are similar to earlier observations in a narrow-gap device [[Mohammadigoushki and Feng \(2012\)](#)].
- (b) The equilibrium position is between the center of the gap and the inner cylinder, at $S_e = 0.36$, the radial coordinate S being defined such that $S = 0$ at the inner cylinder and $S = 1$ at the outer one. Its deviation from the narrow-gap experiments, where the equilibrium is at the center, is due to the non-Newtonian rheology of the foam brought out by the nonhomogeneous shearing in the wide-gap geometry.
- (c) In a xanthan solution representative of the shear-thinning in the foam, a single bubble migrates to an equilibrium position at $S_e = 0.25$, regardless of the initial position, shear rate, or bubble size.
- (d) In a polyacrylamide-based Boger fluid representative of the first normal stress difference in the foam, a single bubble migrates to equilibrium positions close to $S_e = 0.57$, regardless of the initial position and shear rate. The position shifts slightly inward with increasing bubble size. The migration in Boger fluid can be explained quantitatively by the asymptotic theory of [Chan and Leal \(1979\)](#).
- (e) Bubble migration in the foam is the outcome of the competition between its shear-thinning and normal-stress effects. Linear combination of the net migration forces in the shear-thinning and elastic solutions predicts the migration in the foam semiquantitatively.

Thus, the foam made of equal-sized smaller bubbles serves effectively as a non-Newtonian liquid suspending the large bubble. However, this *continuum view* has to be juxtaposed with a *discrete view*. On the one hand, some aspects of foam dynamics can be described as if the foam is an effectively continuous fluid. Examples include the global rheology, often represented by the Herschel-Bulkley model [[Lauridsen et al. \(2002\)](#)], and

the bubble migration summarized above. On the other hand, the foam is a heterogeneous medium and its granularity manifests itself in certain ways. One example is the nonlocal interaction of bubbles that causes the bubble velocity profile to fall below that predicted from the global rheology of the foam as an effective continuum [Katgert *et al.* (2010)]. In the context of lateral migration of bubbles, the thresholds of the shear rate and the bubble size ratio for migration stem from the capillary pressure in individual bubbles [Mohammadigoushki and Feng (2012)]. Therefore, it seems appropriate to recognize a *duality* in foam dynamics. Even though the foam is ultimately heterogeneous, it may be possible and indeed advantageous to disregard the bubble-scale granularity in certain contexts. The granular and continuum attributes of foam should be seen as complementary aspects of a subtle reality.

ACKNOWLEDGMENTS

The authors thank G. M. Homsy for helpful discussions and S. G. Hatzikiriakos for access to rheometers in his lab. H.M. also thanks M. Ansari for many fruitful discussions and his help with N_1 measurements. This study was supported by NSERC, the Canada Research Chair program, and the Canada Foundation for Innovation. Part of this work was done while J.J.F. was a visitor at the Kavli Institute for Theoretical Physics, Santa Barbara, and the author acknowledges support by the National Science Foundation (NSF PHY11–25915).

References

- Aytouna, M., J. Paredes, N. Shahidzadeh-Bonn, S. Moulinet, C. Wagner, Y. Amarouchene, J. Eggers, and D. Bonn, "Drop formation in non-Newtonian fluids," *Phys. Rev. Lett.* **110**, 034501 (2013).
- Bird, R. B., R. C. Armstrong, and O. Hassager, *Dynamics of Polymeric Liquids*, Vol. 1. Fluid Mechanics (Wiley, New York, 1987).
- Bonn, D., and J. Meunier, "Viscoelastic free-boundary problems: Non-Newtonian viscosity vs normal stress effects," *Phys. Rev. Lett.* **79**, 2662–2665 (1997).
- Brenner, H., A. L. Graham, J. R. Abbott, and L. A. Mondy, "Theoretical basis for falling-ball rheometry in suspensions of neutrally buoyant spheres," *Int. J. Multiphase Flow* **16**, 579–596 (1990).
- Chan, P. C. H., and L. G. Leal, "The motion of a deformable drop in a second-order fluid," *J. Fluid Mech.* **92**, 131–170 (1979).
- Chan, P. C.-H., and L. G. Leal, "An experimental study of drop migration in shear flow between concentric cylinders," *Int. J. Multiphase Flow* **7**, 83–99 (1981).
- Estellé, P., C. Lanos, and A. Perrot, "Processing the Couette viscometry data using a Bingham approximation in shear rate calculation," *J. Non-Newtonian Fluid Mech.* **154**, 31–38 (2008).
- Gardiner, B. S., B. Z. Dlugogorski, and G. J. Jameson, "The steady shear of three-dimensional wet polydisperse foams," *J. Non-Newtonian Fluid Mech.* **92**, 151–166 (2000).
- Gauthier, F., H. L. Goldsmith, and S. G. Mason, "Particle motions in non-Newtonian media," *Rheol. Acta* **10**, 344–364 (1971).
- Golemanov, K., S. Tcholakova, N. D. Denkov, K. P. Ananthapadmanabhan, and A. Lips, "Breakup of bubbles and drops in steadily sheared foams and concentrated emulsions," *Phys. Rev. E* **78**, 051405 (2008).
- Herzhaft, B., "Correlation between transient shear experiments and structure evolution of aqueous foams," *J. Colloid Interface Sci.* **247**, 412–423 (2002).
- Kamis, A., and S. G. Mason, "Particle motions in sheared suspensions. XIX. Viscoelastic media," *Trans. Soc. Rheol.* **10**, 571–592 (1966).
- Katgert, G., B. P. Tiche, M. E. Mobius, and M. van Hecke, "Couette flow of two-dimensional foams," *Europhys. Lett.* **90**, 54002 (2010).

- Khan, S. A., C. A. Schnepfer, and R. C. Armstrong, "Foam rheology: III. Measurement of shear flow properties," *J. Rheol.* **32**, 69–92 (1988).
- Kraynik, A. M., and D. A. Reinelt, "Microrheology of random polydisperse foam," Proceedings of XIVth International Congress on Rheology, Seoul, Korea, 2004.
- Krieger, I. M., and H. Elrod, "Direct determination of the flow curves of nonNewtonian fluids. II. Shearing rate in the concentric cylinder viscometer," *J. Appl. Phys.* **24**, 134–136 (1953).
- Labiausse, V., R. Hohler, and S. Cohen-Addad, "Shear induced normal stress differences in aqueous foams," *J. Reol.* **51**, 479 (2007).
- Lauridsen, J., M. Twardos, and M. Dennin, "Shear-induced stress relaxation in a two-dimensional wet foam," *Phys. Rev. Lett.* **89**, 098303 (2002).
- Mohammadigoushki, H., and J. J. Feng, "Size differentiated lateral migration in sheared two-dimensional foam," *Phys. Rev. Lett.* **109**, 084502 (2012).
- Mohammadigoushki, H., and J. J. Feng, "Size segregation in sheared two-dimensional polydisperse foam," *Langmuir* **29**, 1370–1378 (2013).
- Mohammadigoushki, H., G. Gighliotti, and J. J. Feng, "Anomalous coalescence in sheared two-dimensional foam," *Phys. Rev. E* **85**, 066301 (2012).
- Okuzono, T., K. Kawasaki, and T. Nagai, "Rheology of random foams," *J. Rheol.* **37**, 571–586 (1993).
- Ovarlez, G., K. Krishan, and S. Cohen-Addad, "Investigation of shear banding in three-dimensional foams," *Europhys. Lett.* **91**, 68005 (2010).
- Pratt, E., and M. Dennin, "Nonlinear stress and fluctuation dynamics of sheared disordered wet foam," *Phys. Rev. E* **67**, 051402 (2003).
- Wang, Y., K. Krishan, and M. Dennin, "Bubble kinematics in a sheared foam," *Phys. Rev. E* **74**, 041405 (2006).